Nigerian Journal of Environmental Sciences and Technology
(NIJEST)
www.nijest.com
ISSN (Print): 2734-259X | ISSN (electronic): 2734-2603
Vol 7, No. 3 October 2023, pp 435 - 451

Performance Evaluation of Medium Resolution Satellite Images in Bathymetry Estimation for Imo River

Akwaowo U. Ekpa[1], Itoro B. Udoh[*2], and Aniekan E. Eyoh[3]

[1,2,3] Department of Geoinformatics and Surveying, Faculty of Environmental Studies, University of Uyo, Uyo, Akwa Ibom State, Nigeria.
Corresponding author: [*] itoroudoh@uniuyo.edu.ng

https://doi.org/10.36263/nijest.2023.03.0434

ABSTRACT

Medium resolution satellite imageries are prominently used in bathymetry estimation due to high cost of accessing high resolution images and obtaining in-situ data. In this study, Landsat-8 and Sentinel-2 medium resolution satellite images were explored in estimating bathymetry for a section of Imo River with underlying aim of evaluating their performances. Lyzenga log linear and Stumpf log ratio empirical models were adopted. Image pre-processing involved atmospheric correction, cloud masking, sun glint removal and low pass filtering. Comparison with field-based reference depths showed that deepest estimated depth from both satellites images was approximately 10 m compared to 12 m depth obtained from field-based sounding. Coefficient of determination shows that Landsat-8 averagely estimated depths by 57% while Sentinel-2 showed 46% performance. Sentinel-2 had the highest and lowest root mean square error of 1.9 and 1.5 based on Lyzenga and Stumpf model respectively, while Landsat-8 had root mean square error of 1.7 and 1.8 from both models. Fidelity of Sentinel-2 derived bathymetry was greatly impacted by cloud and radiometric effects despite its high spatial resolution and applied corrections. Results of the study revealed that environmental conditions and water body properties have significant impact in satellite bathymetry estimation from medium resolution images.

Keywords: Landsat-8, Sentinel-2, Imo River, Inland Waterway, Satellite-derived Bathymetry

1.0. Introduction

Innovation in space remote sensing and expanding satellite technologies have led to availability of various satellite data for bathymetry estimation. Satellite sensors yield imageries of different spatial resolution and spatial coverage, have inherent benefits and limitations. They are also influenced by terrestrial factors and water body properties (*e.g.* transparency, sediments, seabed rugosity), parameters of measuring device, platform dynamics and operational techniques. The choice of any or a combination of imagery is determined by volume of bathymetric information required, image spatial resolution, nature and extent of study area, coverage and cost (Poti *et al*., 2012; Dierssen and Theberge, 2014).

At different times and for various study locations, performance of satellite images, estimation parameters as well as the estimation algorithm (model) have been undertaken (Casal *et al*., 2018; Cahalane *et al*., 2019; Ahola *et al*., 2020; Evagorou *et al*., 2022). Given recent development in sensors capability, improved resolution and data availability, optical satellite data have increasingly been adopted for bathymetry mapping of inland waters. It is reasoned that optical satellite imagery of various resolutions has capabilities for derivation of bathymetry with reasonable accuracy depending on the nature of the water body, seabed characteristics and study context. However, bathymetry accuracy from optical satellite imagery also depend on spatial resolution, cloud cover, presence of ice, signal transmissivity or visibility in water column, sun elevation angle at time of acquisition as well as date of image acquisition (Casal *et al*., 2018; Ahola *et al.*, 2020). Literature on studies that assess image channel most useful for bathymetry extraction, effect of spatial resolution on estimated bathymetry as well as impact of acquisition geometry on bathymetry abound (Lee, 2012; Tang and Pradhan, 2015). Studies also addressed the issue of estimation parameters whereby specific predictors were used to check specific satellite data performance. El-Sayed (2018) tested the quality of image, calibration procedures and performance of bathymetry estimation algorithm. Water quality parameters like turbulence, optical conditions of turbidity, bottom material and suspended sediment (Kimeli *et al*., 2018; Zandbergen, 2020) and depth of penetration (Ekpa and Ojinnaka, 2018) were considered for accurate bathymetry estimation from optical satellite data.

Categorically, Ahola *et al.* (2020) assessed bathymetric mapping output of imageries with varying spatial resolutions (Landsat-8, PlanetScope, Pléiades-1, Sentinel-2, SPOT, WorldView-2) and reported that high resolution images yielded higher accuracy and produced fine details on larger scale charts. Jaelani *et al. (*2019) reported that Landsat 8 and Sentinel-2A could not yield bathymetry for areas shallower than 8 m and deeper than 13 meters respectively due to poor resolution. Study based on the use of low-resolution Sentinel-2 (10 m) and Landsat-8 (30 m); medium resolution PlanetScope (5 m); and high resolution Pléiades (2 m) and Worldview-2 (1.31 m) revealed that low resolution datasets gave reduced detail of seabed features. As reported, depths less than 12 m had low accuracy of information representation due to limited sensing capability while results in mid-depth ranges (4–10 m) gave a higher accuracy with greater details as a result of the high mapping power of optical sensor within this region (Ahola *et al.*, 2020). The study also revealed that images with more spectral bands offer better mapping potentials even for waters with high turbidity.

Given that satellite images covering coastal regions and areas of massive water body are usually affected by coastal climatic factors such as cloud, wind, and waves including inherent optical and apparent optical properties, there is need to evaluate the suitability of freely available medium resolution satellite image in estimating inland waterway bathymetry. Inland waterways are “the most accessible and important resource” among the water resources available to man (Revenga and Kura, 2003). Inland waterways are navigable body of water (rivers, lagoons, canals, lakes, watercourses, inlets and bays *etc.*) located within a country’s territory, suitable for navigation. They are laden with many economic significances including fishing, water transport, oil and gas exploration, recreation, eco-tourism, industrial water supplies, and irrigation (Revenga and Kura, 2003; Chukwuma, 2014; Said *et al*., 2017). Bathymetry of this ecosystem will facilitate sustainable development and improvements within the fringes (Vanderstraete *et al*., 2003; Chukwuma, 2014; International Hydrographic Organization-IHO, 2019). As ecologically dynamic environment, inland waterways are usually impacted by turbidity and sediment through human related activities, floods, vegetation, wrecks, etc., and parameters for bathymetry estimation should be selected to suit the peculiarity of the ecosystem. A performance assessment of Landsat-8 and Sentinel-2 medium resolution satellite images freely available and commonly used for bathymetry estimation was undertaken. This study covers a section of Imo River - an inland waterway in South-South Nigeria with sparse hydrographic data.

2.0 Methodology

2.1 Study Site

Imo River is one of the major rivers in Nigeria and an inland waterway in the south. With the source at Udi Hill, Imo State, Imo River drains an area of 8,288 km^2 and cover a floodplain (wetland) of 26,000 hectares. The river flow across four states (Imo, Abia, Rivers and Akwa Ibom) and empties into Atlantic Ocean through the Bight of Bonny. Imo River is a major landmark and serves as natural boundary between Akwa Ibom and Rivers States in South-South Nigeria. The river lies between Latitudes 4° 30'N and 5° 00'N and Longitudes 7° 10'E and 7° 45'E with a total length of 225.3 km (Oyo-Ita and Oyo-Ita, 2017).

Imo River lies within equatorial rain forest belt with characterized stormy rains in the rainy season (April to October) and mild weather conditions during dry season (November to March). The region has high relative humidity throughout the year (Amadi *et al*., 2016). Temperature ranges between 26.6° C in the rainy season to 31.6° C in the dry season (Okorie and Nwosu, 2014). The River ecosystem is estuarine swamp forest of nipa palm, shrubs, and mangrove vegetation. Imo River lies within Imo drainage system and underlain on Benin groundwater system and has an estuarine ecosystem with relative level of turbidity due to high sediment load. The section of focus was the lower course with Longitudes 07° 30' 30" and 07° 33' 00"E and between Latitudes 04° 35' 00" and 04° 32' 00"N (Figure 1). The river section is located within the borders of Akwa Ibom (to the East) and Rivers State (on the West).

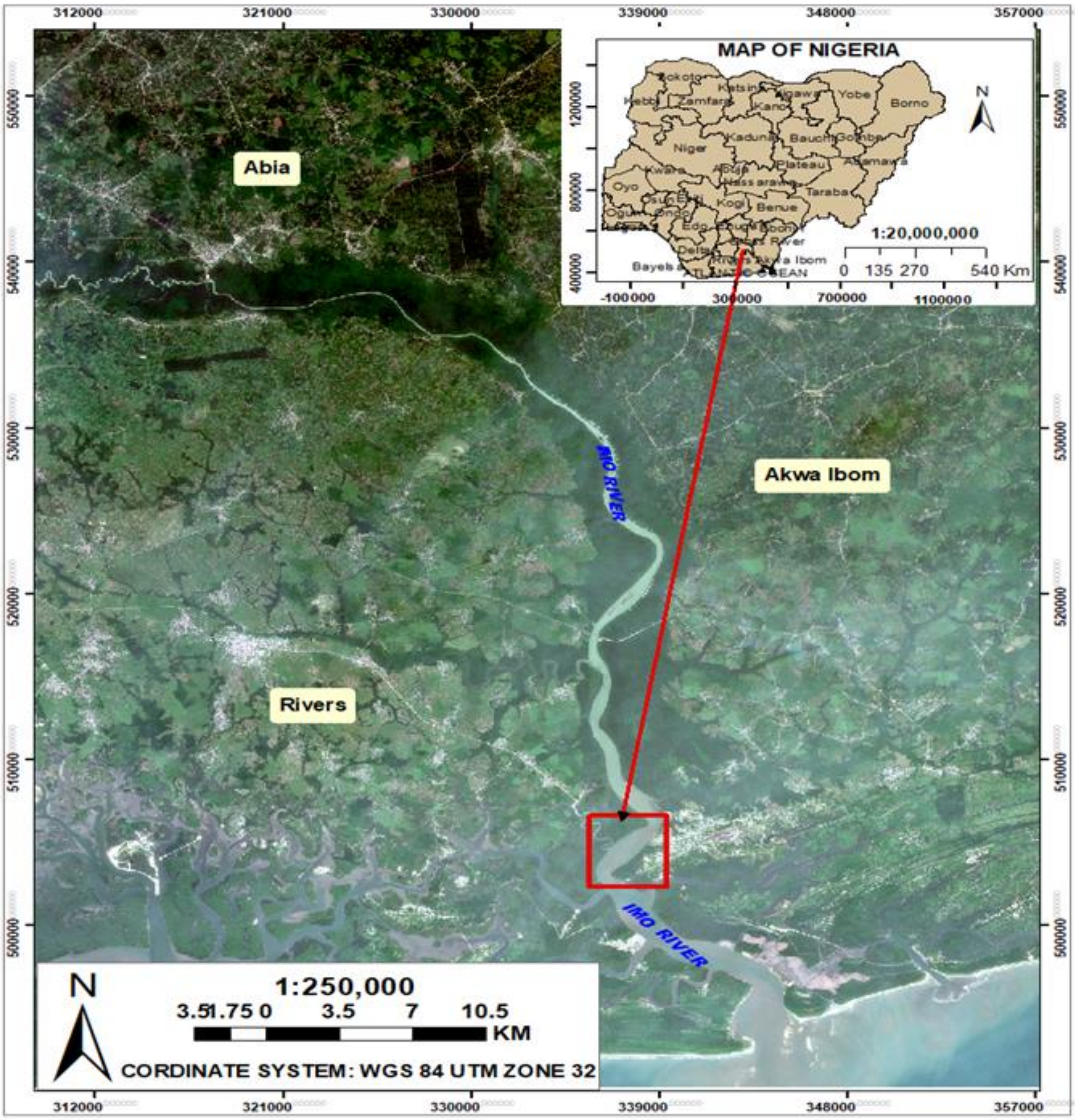

Figure 1: Image Map Showing Study Site

2.2 Data Acquisition

Two sets of medium resolution satellite images, Landsat-8 OLI and Sentinel-2 MSI were used for bathymetry estimation. Landsat-8 OLI images included level-1 (L1TP) and level-2 (L2SP) of February 18, 2021 and level-2 image of December 19, 2021. These were downloaded from https://earthexplorer.usgs.gov based on 187/057 path/row World Reference System (WRS). Two Sentinel-2A level- 2 (MSIL2A) images captured on January 24, 2021 and December 20, 2021 used were downloaded from https://scihub.copernicus.eu. Specification for image download included full coverage of the river section, clarity and minimum cloud cover. Images acquired in dry season where climatic conditions were similar to the period of sounding data acquisition were selected. These are shown in figure 2 (i) –(v).

A (i) Sentinel-2A of Jan. 24, 2021 (ii) Sentinel-2A of Dec. 20, 2021

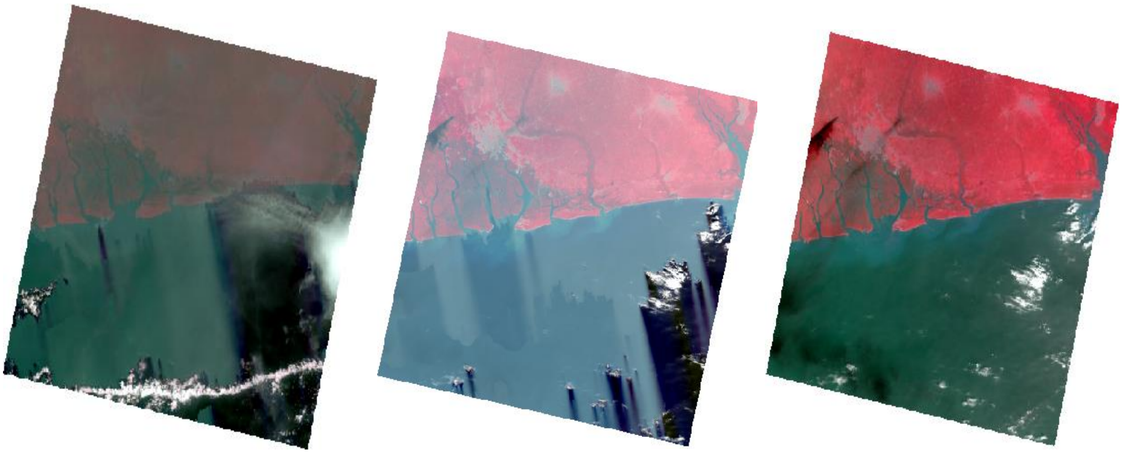

B (iii) Landsat-8 level 2 image image of Feb. 18, 2021 (iv) Landsat-8 level 2 image of Dec. 19, 2021 (v) Landsat-8 level 2 of Dec. 19, 2021

Figure 2 (i) –(v): Satellite Images Used in the Study

Two of the images (with Asterix in table 1) were acquired at the onset of dry season while others (marked a, b, c) were sensed in the middle of dry season period. Influence of tide on the dates and time () of satellite image acquisition was noted and presented in table 1 while characteristics of selected image bands used are presented in table 2.

Table 1: Predicted Water Levels Based on Image Acquisition Date

Satellite sensor	Satellite data	Date of image acquisition	Time of image acquisition (GMT)	Predicted tide (m)
Sentinel-2 MSI	*S2A_MSIL2A	24/01/2021	12:07:07	1.005
	[a] S2A_MSIL2A	20/12/2021	12:03:47	0.465
	[b]LC08_L1TP	19/12/2021	09:45:31.4714750Z	0.831
Landsat-8 OLI	*LC08_L2SP	18/02/2021	09:45:15.3232880Z	2.007
	[c]LC08_L2SP	19/12/2021	09:45:31.4714750Z	0.831

GMT= Greenwich Mean Time

Table 2: Characteristics of Satellite Image

Sentinel-2			**Landsat-8**		
Bands	Wavelength (μm)	Resolution	Bands	Wavelength (μm)	Resolution
02-Blue	0.448 – 0.546	10 m	2-Blue	0.450 – 0.515	30 m
03-Green	0.538 – 0.583	10 m	3-Green	0.525 – 0.600	30 m
04- Red	0.646 – 0.684	10 m	4- Red	0.630 – 0.680	30 m
8A- Broadband Near infrared	0.763 – 0.908	10 m	5- Near infrared	0.845 – 0.885	30 m

Source: El-Mewafi *et al.* (2018); Zandbergen (2020) and Schmitt (2020)

Field data used for calibration of estimation model and validation of estimated bathymetry was obtained on January 24, 2021 using South SDE-28 Single Beam Echosounder integrated with Hi Target DGPS GNSS Receiver. The echo sounding measurement was carried out within the same year of image acquisition (see table 2 for reference).

2.3 Methods

The processes carried out included image pre-processing; application of bathymetry algorithm and depth estimation; and validation of satellite derived bathymetry.

2.3.1 Image pre-processing

i. Atmospheric and radiometric correction: Atmospheric correction is the removal of scattering and absorption effects caused by particles and other matters present in the atmosphere that negatively impacts on image at the time of acquisition (Gabr *et al*., 2020; Hashim *et al*., 2021). It also involves the 'conversion of relative radiance into calibrated reflectance' (Muzirafuti *et al.*, 2020). For Sentinel-2 and Landsat-8 level-2 images used, atmospheric correction was not applied as they were downloaded geometrically and radiometrically rectified, atmospheric correction were only applied on Landsat-8 Level-1C product. Case 2 Regional Coast Colour processor (C2RCC), available on Sentinel Application Platform (SNAP) toolbox, provided by European Space Agency was applied. C2RCC is an image-based atmospheric correction algorithm that uses inputs from pre-calculated look up tables usually derived from the image (Casal *et al*., 2018; Caballero and Stumpf, 2020). C2RCC is water focused processor with the functionality of atmospheric disturbances, sun glint and adjacency effect (Casal *et al*., 2019). This processor is embedded in SNAP as C2RCC S2-MSI Processor.

Radiometric correction was applied to correct errors in image radiance and convert image digital numbers to spectral radiance. Radiometric corrections applied included normalization, low pass filtering, cloud and sunglint correction. Normalization is the process of scaling pixel values in DN to surface reflectance by applying a scale factor. Surface reflectance is a unitless physical quantity of value usually between 0.0 and 1.0 (S2-PDGS-MPC-L2A-PFS-V14.2, 2017). For Landsat-8 level-1 and Level-2 image, the scale factors were 0.0001 and 0.0000275 + -0.2 respectively (LSDS-1619, 2022). These were applied to the images before extracting water pixels for bathymetry estimation. Normalization of Sentinel-2 MSI Level-2A was by applying the quantization value of 10000 based on the relationship; SR = DN / 10000 (S2-PDGS-MPC-L2A-PFS-V14.2, 2017).

Low pass filtering is the process of smoothening anomalous cells by passing 3 × 3 kernel size filter over the image bands. This was executed using 'Spatial Analyst Tools' (Neighborhood – Filter) in ArcGIS. Cloud mask correction was applied only on Sentinel-2 image of January 24, 2021. Clouds act as artefacts on the image and obstruct reflection from the river from reaching the satellite sensor (Zandbergen, 2020). Masking of cloud was carried out alongside with separation of water body from land based on NIR threshold method. Sunglint correction was applied to Sentinel-2 of January 24, 2021 and December 20, 2021 and Landsat-8 of February 18, 2021 using Hedley *et al.* (2005) method as expressed in Equation 1. This method works on the principle that samples or selected pixels in the visible band are included in 'a linear regression with NIR values. Established linear regression among image pixels as defined by the slope of the regression line for a particular band was used to predict the brightness for other pixels (Holman, 2020). The generalized algorithm to correct all image pixels of sun glint in an image band 'i' according to Hedley *et al.* (2005) is given:

$$R'_i = R_i - b_i\,(R_{NIR} - Min_{NIR}) \qquad (1)$$

Here, R'_i is sun glint-corrected pixel, R_i is pixel value in visible band i, b_i is regression slope for visible band i, R_{NIR} is pixel value of NIR band while Min_{NIR} is minimum reflectance value of NIR band. A polygon was created over the NIR band. After cloud masking, the masked-out portions on the Sentinel image were filled with corresponding values of sentinel 2 level-2 acquired on 20 December, 2021. For all the images, float and low pass filter processes were applied to each band to remove speckle noise and enhance the radiance of the pixels for precise feature extraction (GEBCO Cookbook, 2019; Saeed *et al*., 2021). This was done before separating water pixels from land.

ii. Spatial sub-setting and separation of water body from land: Prior to spatial filtering, image bands were clipped to area of interest to reduce processing time and storage space. Subsequently, pixels containing only water or covering the study area was masked out for further processing. This usually eliminates contamination of water pixels by land and other objects. NIR threshold method adopted in GEBCO Cookbook (2019) was used. A line profile stretching from land into the water portion of each image was created over NIR band. A graph of the line profile was then created to display the change in reflectance values of pixels along the line. Since pixel values of land and cloud mask had higher reflectance than water pixels, there was a sharp drop in the profile line at the land/water boundary. The value at this point was recorded as the threshold value.

Next, this value was used as a condition using the “Set Null” tool of ArcGIS to separate water pixels from others. NoData value was assign to pixels with reflectance higher than the threshold (*e.g.* 0.08 for Sentinel-2). Figure 3 presents the profile line over NIR band, profile graph and ‘Set Null’ dialog box in ArcGIS. This procedure was repeated for all images to extract water pixel reflectance.

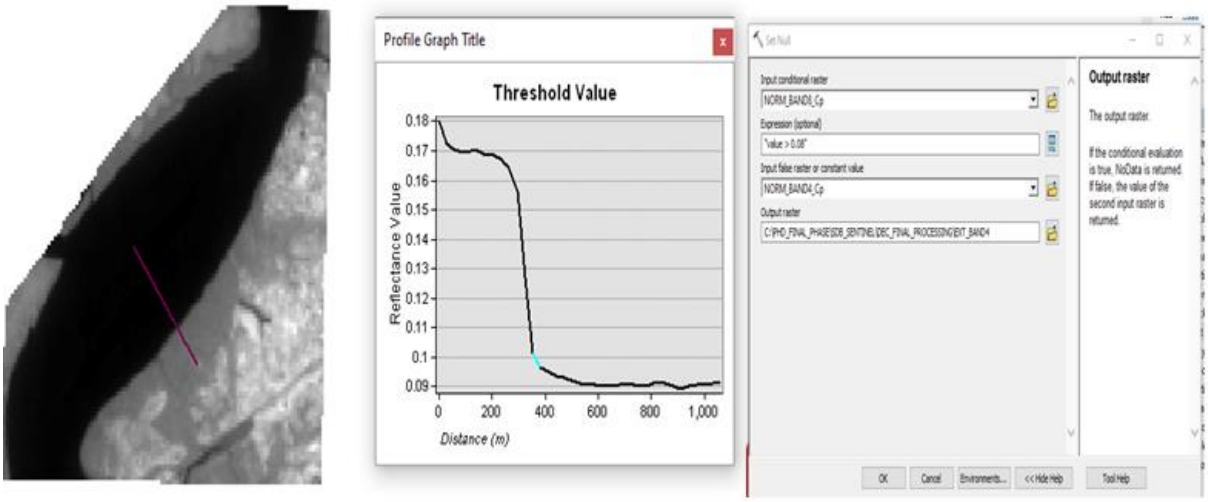

Figure 3: Profile Line Over NIR Band, Profile Graph and ‘Set Null’ Dialog Box in ArcGIS Adopted in Masking Out Cloud and Land from Water Body

2.3.2 Application of bathymetry algorithm and depth estimation

Bathymetry algorithm used in this study were the Stumpf *et al*. (2003) log ratio and Lyzenga *et al*. (2006) log linear models. Application of bathymetry algorithm and depth estimation involved calculation of relative bathymetry using different band reflectance, regression analysis, computation of SDB and vertical referencing. For effective performance and suitability evaluation of image bands in bathymetry estimation within the context of the study, bands blue, green and red as well as the combination of the three bands were adopted. This was due to the fact that although blue and green bands are strongly advocated and widely used for bathymetry estimation (Traganos *et al*., 2018; Amrari *et al*., 2021), in a separate study, Khondoker *et al*. (2017) and Liu *et al*. (2021) portrayed that short wavelength bands (blue and green) are not very appropriate for turbid waters due to their sensitivity to inherent optical properties (IOP). Besides, Khondoker *et al*. (2017) advocated that red and infrared long wavelength bands are ideal for bathymetry estimation while short wave infra-red 1 (band 6) of Landsat-8 was also recommended for bathymetry estimation (GEBCO Cook Book, 2019). In a later study, Arabi *et al*. (2020) proved that red band strongly correlate with water depth and not very sensitive to IOPs.

i. Bathymetry estimation based on Stumpf model: this method works on the assumption that long wavelengths are attenuated more rapidly in water with increase depth than short wavelengths. And that the ratio between short wavelength band and long wavelength band will increase with changes in depth than by bottom albedo. Natural logarithmic transformation of the ratio will linearize the relationship as a function of depth (Rossi *et al*., 2019). Stumpf model is more stable and is effective over turbid waters and water bodies of variable bottom (Jagalingam *et al*., 2015). Stumpf model is expressed as:

$$Z = m_1 \frac{\ln(n * R_W\ (\lambda_i))}{\ln(n * R_W\ (\lambda_j))} - m_o \qquad (2)$$

Z = satellite derived bathymetry; R_w = observed water radiance; $\lambda_{i,j}$ = wavelength bands; m_0 = offset value for zero depth (when Z = 0) ; m_1 = tunable constant to scale the ratio to depth; n = fixed constant. In the present study, the two models were insensitive to values of n and thus the n constant was not applied.

Different band ratios were calculated to obtain optimum band combination for retrieving bathymetry. These included B2/B3, B2/B4 and B3/B4. Taking the natural logarithm of the band ratios gave relative bathymetric (RB) values. RB outputs (raster values) were employed in least squares regression analysis with 30% of randomly selected reference depths to obtained regression coefficients (m_1 and m_0). Satellite derived bathymetry SDB was obtained by applying the coefficient to RB according to equation (Equation 2). Predicted water level was applied on SDB according to date and time of image acquisition for vertical reference to MWL datum.

ii. Bathymetry estimation based on Lyzenga model: Lyzenga model assumes that water surface reflectance is an exponential function of depth and that by taking a logarithmic transformation; a linear relationship could be established between surface reflectance and water depth. Image radiance are linearized by natural logarithm while coefficients are used to train the model through linear and multiple least square regression least square (Traganos *et al*., 2018; Gabr *et al*., 2020; Zandbergen, 2020). The generalized form given by Gabr *et al*. (2020) and expressed by Equation 3 was adopted.

$$Z = a_0 + \sum_i^n a_i X_i \qquad (3)$$

From equation 3, $X_i = \ln[nR_i(\lambda_i)]$ (4)

Equation 4 represent natural log of radiometric and atmospheric corrected image bands. Linear regression was applied to single bands (2, 3, and 4) while multiple regression was used for multi-band combinations (2-3, 2-4, 3-4, and 2-3-4).

From equations 3 and 4, Z = satellite-derived bathymetry; X_i = log transformed reflectance of band i; $R(\lambda_i)$ = observed reflectance in i band; a_0 and a_i = regression coefficients (intercept and slopes). In equation 3, n represent number of image bands adopted in bathymetry estimation. For equations 4, n denote the tuning constant.

2.3.3 Validation of satellite derived bathymetry

To validate estimated depths, randomly selected 70% of the 1969 Single Beam Echo Sounding (SBES) depths were used. Corresponding depth values of SBES and Satellite-Derived Bathymetry (SDB), were extracted and compared based on root mean squared error (RMSE), lowest depth, mean depth and deepest depth values, and coefficient of determination (R^2).

3.0 Result and Discussion

Results of the bathymetry estimation process are presented in this section. Figures 4 to 8 are depth models depicting the bathymetry based on different band ratios and band combinations from the five satellite images. Bathymetry from Landsat-8 level-2 of February 18, Landsat-8 level-1 and Landsat-8 level-2 of December 19, 2021 are presented in figures 4, 5 and 6 respectively. Figures 7 and 8 respectively depict results obtained from Sentinel-2 level-2 images of January 24 and December 20, 2021.

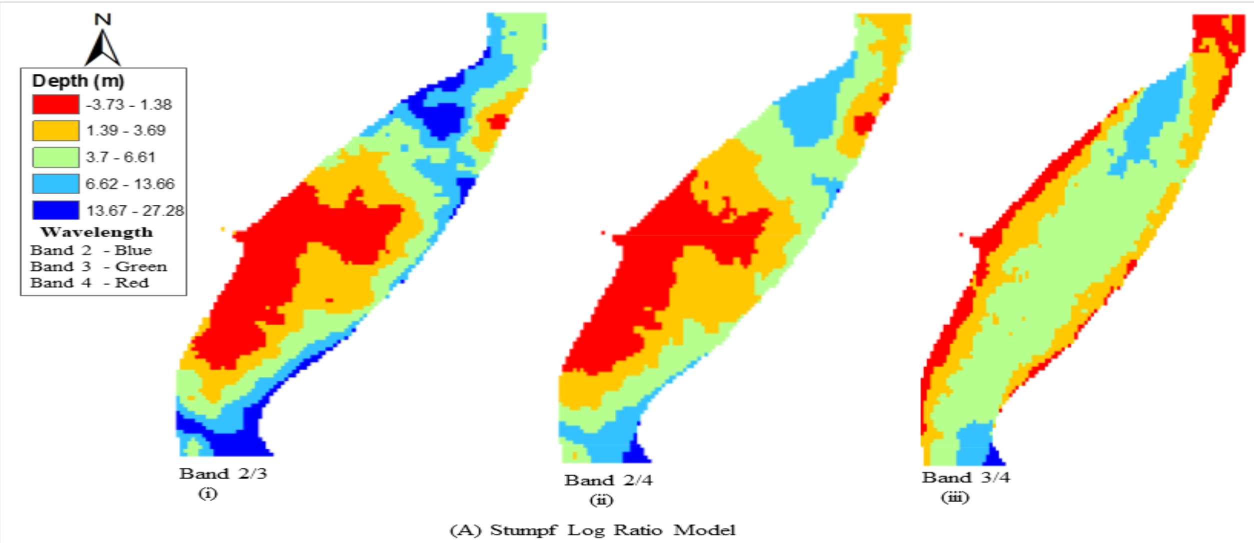

Figure 4A: Estimated Bathymetry from Landsat-8 level-2 of February 18, 2021 Based on Stumpf Model

Figure 4A shows bathymetry generated from Landsat-8 level-2 of February 18, 2021 based on Stumpf's model. Estimated depth ranges were far beyond the in-situ depths (-3.73 m to 27.28 m) for the sounded location. However, the best SDB was generated by the green/red band ratio [Figure 4A (iii)]. Although depths in the north section were correctly derived as deeper depths (light blue), these values were far beyond the reference depths.

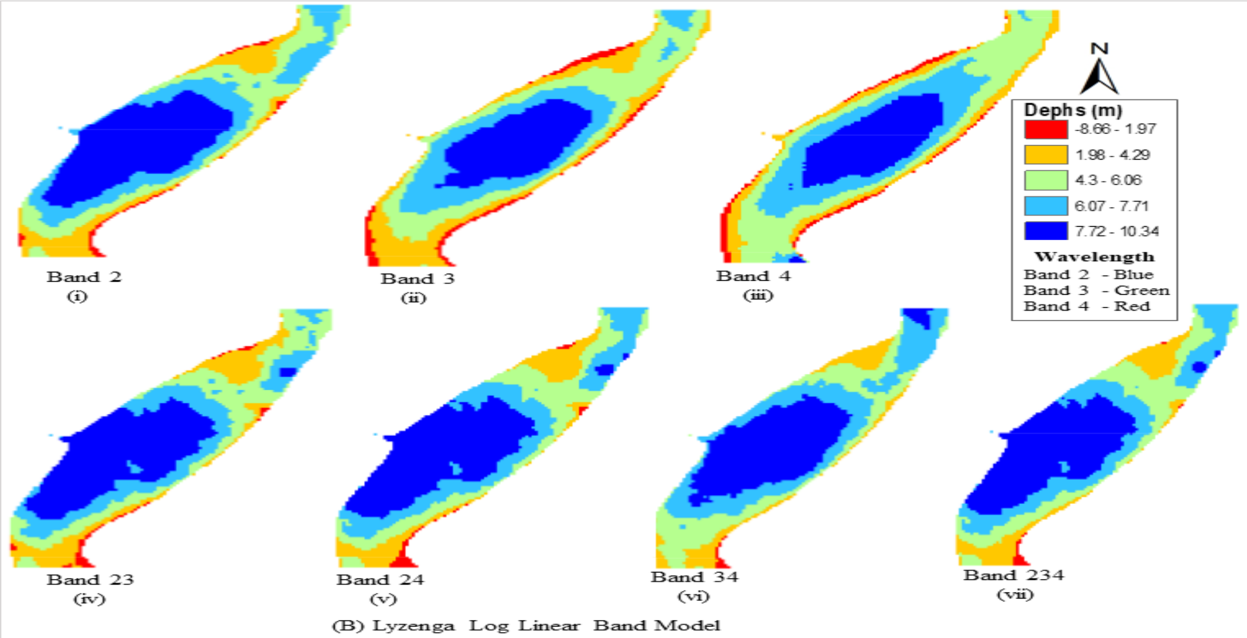

Figure 4B: Estimated Bathymetry from Landsat-8 level-2 of February 18, 2021 Based on Lyzenga Model

In figure 4B, estimated bathymetry based on Lyzenga's model from Landsat-8 level-2 of February 18, 2021, shows that the river is deeper (deep blue) within the central portion of the study area. Based on the in-situ data, this result is incorrect. Although part of the middle section is deep, the fringes are shallow, and not as portrayed in figures 4B (i), (iv), (v), (vi) and (vii). Nevertheless, figures 4B (ii) and (iii) have values that correlate fairly with in-situ depths, but, values within the meandering section (neck-like portion in the north region) were underestimated. Generally, depths above extinction depth based on this image (Landsat-8 level-2 of February 18, 2021) were under estimated by 12.31 m while depth within the extinction value were over estimated by 7.04 m. This was applicable to all estimated depths from Stumpf's (Figure 4A) and Lyzenga's models (Figure 4B).

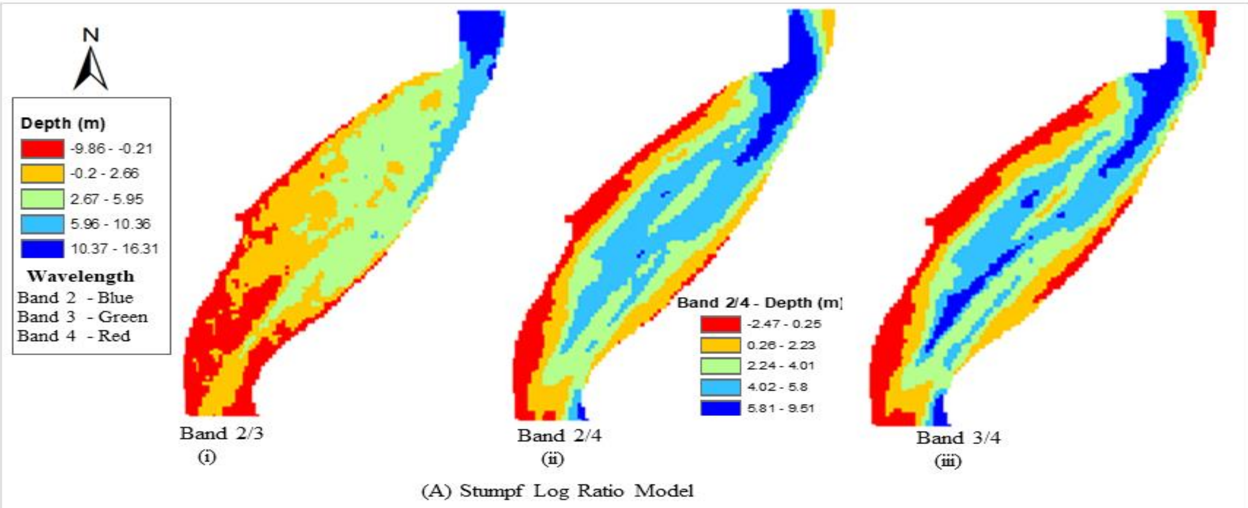

Figure 5A: Estimated Bathymetry from Landsat-8 level-1 of December 19, 2021 Based on Stumpf's Model

Figure 5A is estimated bathymetry from Landsat-8 level-1 of December 19, 2021 (L1TP) using Stumpf's model. The figure (5A) revealed that shallow depths (orange and red colour) are obtainable within the fringes of the river. This correspond with in-situ depths except for results obtained from the green/blue ratio [Figure 5A (i)], which extends shallow depths into regions which are naturally deep. This result [Figure 5A (i)] underestimated shallow depths by about 9.00 m and overestimated deeper depths by about 10 m.
However, bathymetry from blue/red ratio [Figure 5A (ii)] and green/red ratio [Figure 5A (iii)] correlated better with in-situ depths. Since blue/red ratio [Figure 5A (ii)] produced depths deeper than the green/red ratio [Figure 5A (iii)], it was adjudged the best from the satellite data.

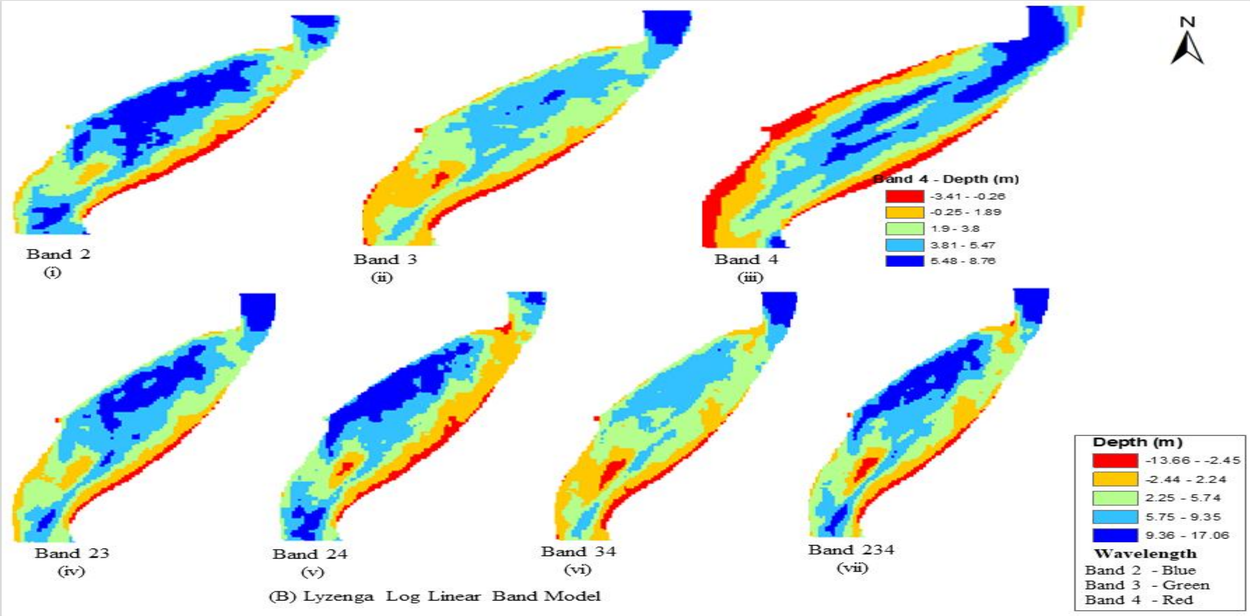

Figure 5B: Estimated Bathymetry from Landsat-8 level-1 of December 19, 2021 Based on Lyzenga Model

Figure 5B is a graphical representation of bathymetry generated from Landsat-8 level-1 of December 19, 2021 based on Lyzenga algorithm from different band combinations. Figure 5B (iii) gave the optimum results as region of shallow depths (orange and red) clearly portray what is obtainable in the river. Figures 5B (i), (iv), (v) and (vii) present shallow depths as being deep (blue colour) contrary to field fact. For figure 5B (ii), shallow depths were underestimated by about 11 m and deeper depths over estimated by about 10 m.

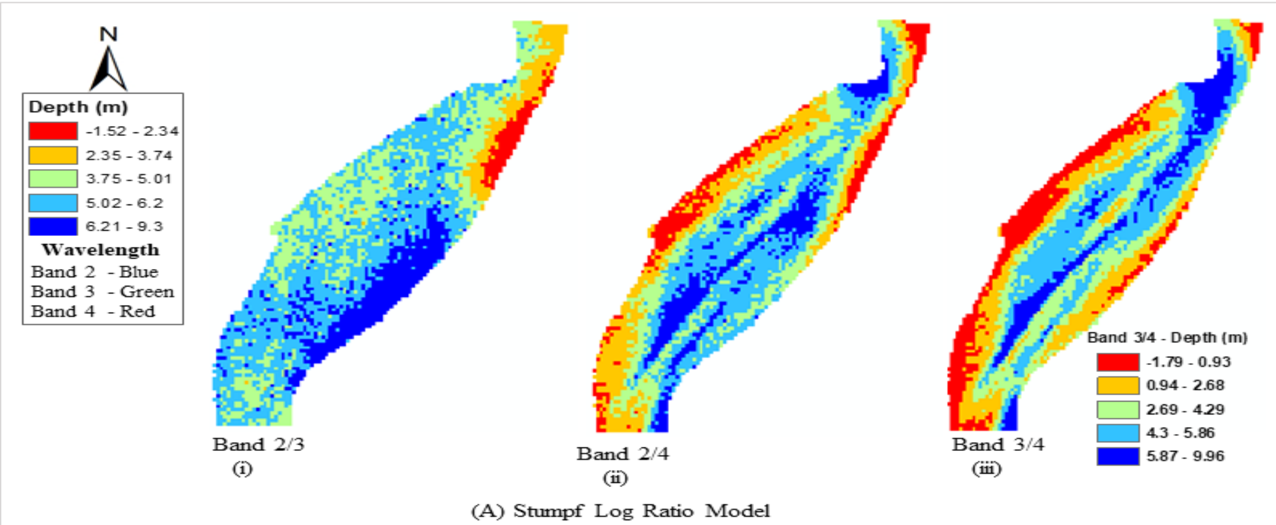

Figure 6A: Estimated Bathymetry from Landsat-8 level-2 of December 19, 2021 Based on Stumpf Model

Bathymetry estimated using Landsat-8 level-2 of December 19, 2021 (L2SP) presented in figure 6A revealed that result from green/red band ratio [Figure 6A (iii)] was the optimum output as it correlated with in-situ depths. Although the depths were generally underestimated by about 3 m for deeper depths (blue colour) and 0.6 m for shallow depths (red colour), it was better than others [Figures 6A (i) and (ii)]. The blue/green ratio produced the worst output as shallow region (South-West) was estimated as deep waters (blue colour) [Figure 6A (i)].

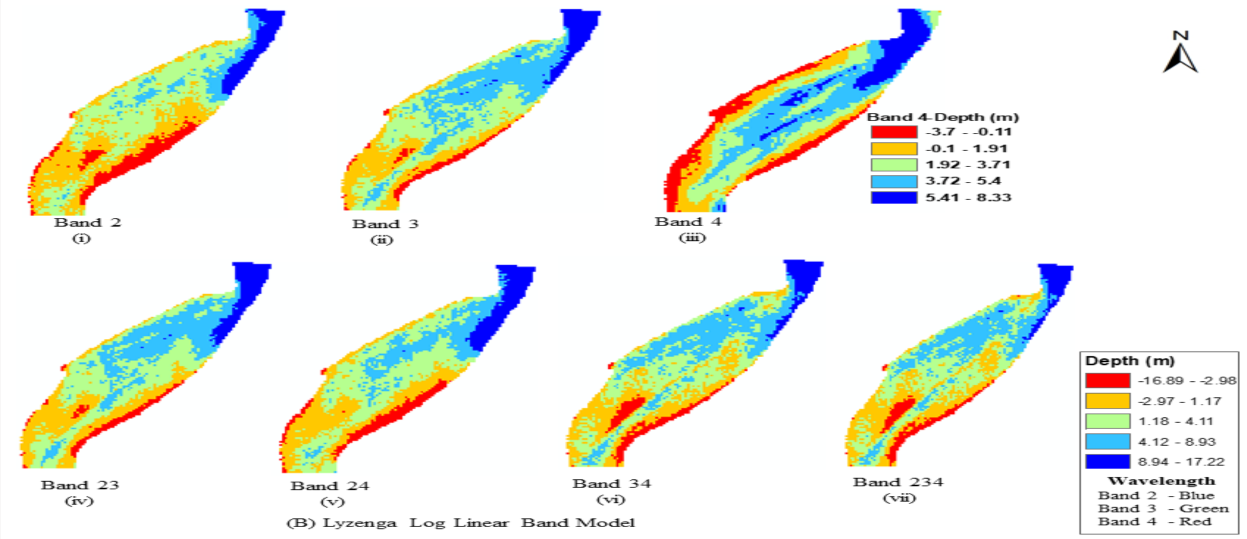

Figure 6B: Estimated Bathymetry from Landsat-8 level-2 of December 19, 2021 Based on Lyzenga Model

Results based on Lyzenga's model from Landsat-8 level-2 of December 19, 2021 (L2SP) presented in figure 6B revealed that outputs from bands 2, 3 as well as bands 23, 24 and 234 combination were noisy and at variant with in-situ depths. Except for band 4 [Figure 6B (iii)] which produced fair output where deeper depths were underestimated by 4.63 m.

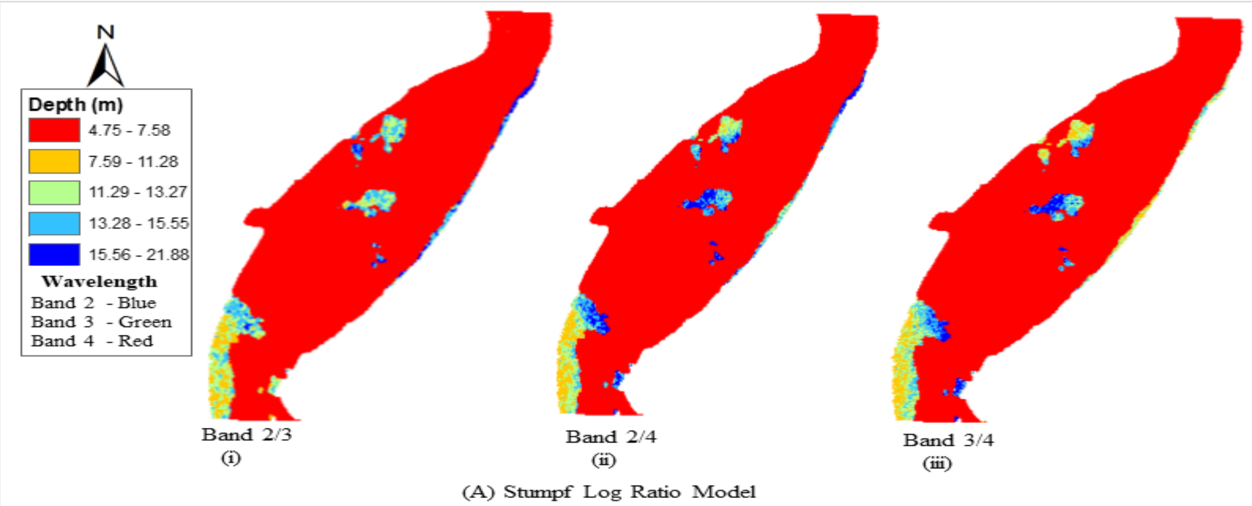

Figure 7A: Estimated Bathymetry from Sentinel-2 level-1 of January 24, 2021 Based on Stumpf Model

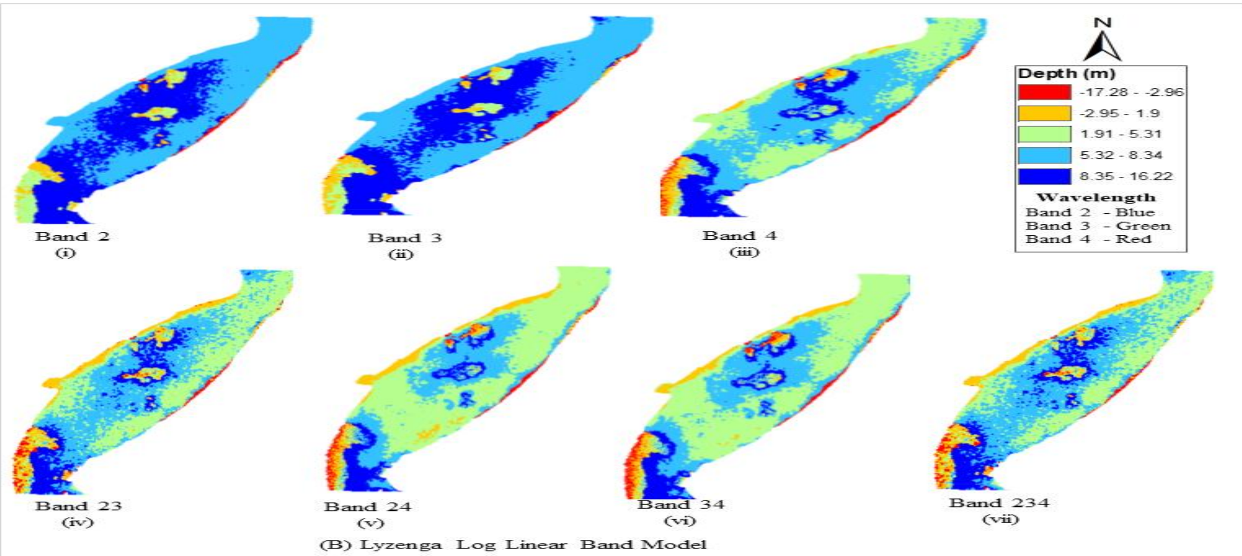

Figure 7B: Estimated Bathymetry from Sentinel-2 level-1 of January 24, 2021 Based on Lyzenga Model

Figure 7A is the estimated bathymetry from Sentinel-2 level-2 of January 24, 2021 using Stumpf *et al*. (2003) ratio model. It shows that output from the satellite were generally noisy and ill-conditioned as the river was portrayed to be generally very shallow (red colour) contrary to sounding result and field-based findings. For Lyzenga's linear model, the output from Sentinel-2 Level-2 of January 24, 2021 (Figure 7B), indicated that only very minimal portions of the river were shallow (orange and red), while a vast section were deep (sky blue and deep blue). Regions where cloud were masked out (and filled with pixels from Sentinel-2 of December 20, 2021) generally gave shallow depths.

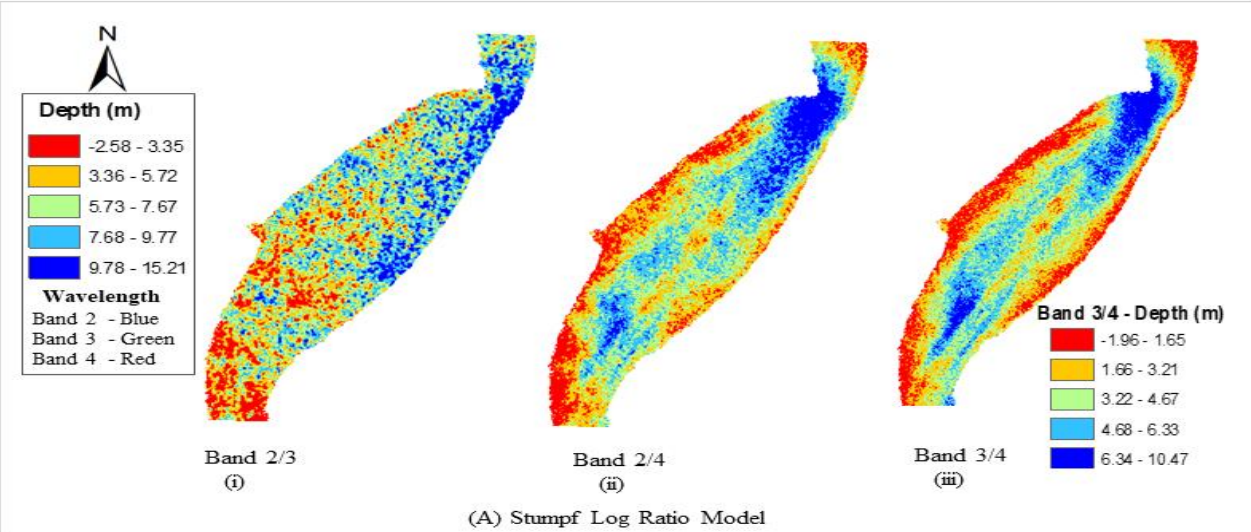

Figure 8A: Estimated Bathymetry from Sentinel-2 level-2 of December 20, 2021 Based on Stumpf Model

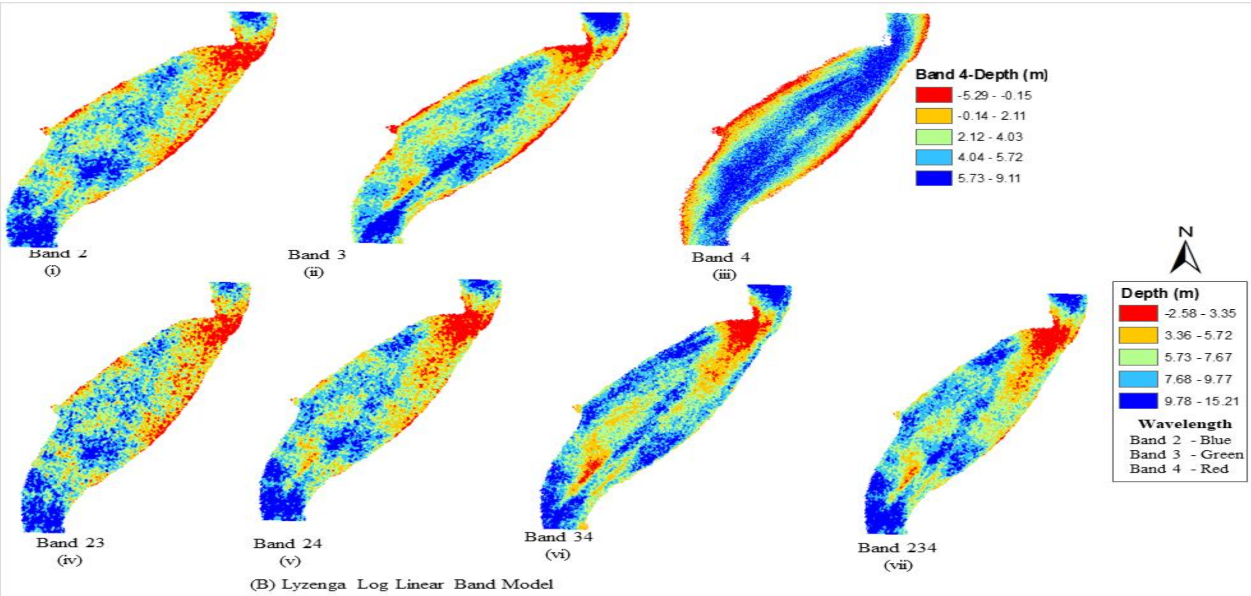

Figure 8B: Estimated Bathymetry from Sentinel-2 level-2 of December 20, 2021 Based on Lyzenga Model

Figure 8A revealed bathymetry depth ranges between -2.58 and 15.21 m from Sentinel-2 level-2 of December 20, 2021 which fairly correlate with in-situ depths. However, the blue/green ratio [Figure 8A (i)] gave noisy output with no clear distinction between points of average depth of 7.68 to 8.77 m (sky blue) and low depth of 5.73-7.67m (lemon shade). Figure 8A (iii) gave a better presentation of the river and was marked as the best output from Sentinel-2 level-2 of December 20, 2021. Estimated bathymetry from Sentinel-2 level-2 of December 20, 2021 based on Lyzenga model (Figure 8B) shows that the outputs were generally noisy which could be attributed to the effect of sunglint and cloud at the time of image acquisition. There were no distinct depth variations, except for result from the red band (4) [Figure 8B (iii)]. Comparatively, regions of low depth values based on in-situ data were estimated as deep waters, while region of deep waters were estimated as shallow depths.

Results from Landsat-8 level-2 of February 18 and Sentinel-2 Level-2 of January 24, 2021 were ill conditioned and therefore not considered for further analysis. Whereas, bathymetry estimated from Landsat-8 level-1 of December 19, 2021 (L1TP), Landsat-8 level-2 of December 19, 2021 (L2SP) and Sentinel-2 level-2 of December 20, 2021 (MSIL2A) were adjudged more consistent and reliable. Statistical and visual analysis presented showed that for Stumpf model, the optimum results from Landsat-8 level-2 of December 19, 2021 and Sentinel-2 level-2 of December 20, 2021 were from the green/red band ratio [Figure 6A (iii) and Figure 8A (iii) respectively]. Whereas for Landsat-8 level-1 of December 19, 2021, the blue/red ratio yielded the best result [Figure 5A (ii)]. For Lyzenga model, the optimum results were obtained from red band for all the satellite data [Figure 5B (iii), Figure 6B (iii), and Figure 8B (iii)]. Statistics of these results were adopted and further evaluated based on the research objectives. Extracted depth information were exported into Excel spreadsheet and appropriate formulae used to execute the statistical analysis. Results are presented in tables 3, 4, and 5.

Table 3: Statistics of Landsat L1TP Bathymetry

	SDB -blue/green	**SDB-blue/red**	**SDB-green/red**	**SDB-red**
RMSE	2.5	1.7	2.1	1.8
Lowest Residual	-5.24	-0.27	0.91	0.42
Highest Residual	6.87	1.96	1.93	2.41
Lowest depth (m)	-9.86	-2.47	-1.72	-3.41
Highest depth (m)	16.31	9.51	9.38	8.76

Table 4: Statistics of Landsat L2SP Bathymetry

	SDB -blue/green	**SDB-blue/red**	**SDB-green/red**	**SDB-red**
RMSE	3.1	2.4	1.8	1.7
Lowest Residual	-1.61	-2.44	-2.54	-2.32
Highest Residual	9.36	8.23	6.63	5.56
Lowest depth (m)	-1.49	-1.52	-1.79	-3.70
Highest depth (m)	8.54	9.3	9.96	8.33

Table 5: Statistics of Sentinel MSIL2A Bathymetry

	SDB -blue/green	**SDB-blue/red**	**SDB-green/red**	**SDB-red**
RMSE	2.7	1.5	1.5	1.9
Lowest Residual	-6.23	-1.04	1.41	0.83
Highest Residual	10.61	5.36	3.34	5.44
Lowest depth (m)	-3.71	-2.57	1.96	-5.29
Highest depth (m)	12.02	11.11	10.47	9.11

From table 3, bathymetry from Landsat L1TP for blue/red ratio was the most statistically significant with root mean square error (RMSE) of 1.7 compared to that of the blue/green (2.5) and green/red ratio (2.1). This was adopted as the best result for Stumpf log-ratio model and considered most appropriate bathymetry for the river. For Landsat-8 L2SP (Table 4), bathymetry of green/red ratio had the least RMSE of 1.8 compared to blue/green (3.1) and blue/red ratio (2.4). The green/red ratio bathymetry of Sentinel MSIL2A also had the least RMSE and residual (Table 5). Thus, bathymetry of green/red ratio for Landsat-8 L2SP and Sentinel MSIL2A were marked as the most appropriate bathymetry for the river. For Lyzenga linear band model, bathymetry from the red band was adopted as the best based on previous analysis and comparison. Statistics of SBD considered as optimum are presented in Table 6.

Table 6: Statistics of Validation Result Based on Landsat-8 L1TP, L2SP and Sentinel-2 MSIL2A Estimated Depth

Parameters	**SBES**	**SDB - Landsat L1TP**		**SDB - Landsat L2SP**		**SDB - Sentinel MSIL2A**	
		Lyzenga model (SDB_{RED})	**Stumpf model (SDB_{BR})**	**Lyzenga model (SDB_{RED})**	**Stumpf model (SDB_{GR})**	**Lyzenga model (SDB_{RED})**	**Stumpf model (SDB_{GR})**
Std. Dev.	2.1	1.7	1.8	1.7	1.7	1.6	1.9
RMSE		1.8	1.7	1.7	1.8	1.9	1.5
R^2		0.53	0.62	0.58	0.55	0.30	0.62
Average depth (m)	4.68	3.09	3.05	2.87	3.38	4.03	3.71
MIN depth (m)	-0.66	-3.41	-2.47	-3.70	-1.79	-5.29	1.96
MAX depth (m)	12.96	8.76	9.51	8.33	9.96	9.11	10.47

The study results reveal that depths from Sentinel MSIL2A based on Stumpf model had the deepest depth of 10.47 m and shallowest depth of -5.29 m based on Lyzenga model. Averagely, computed standard deviation of estimated depths were within the same range but for Sentinel MSIL2A which showed the least standard deviation (1.6 m) for the red band and highest (1.9 m) for the green/red ratio. The standard deviation of 1.6 m implies that the depths were closely clustered around the mean depth. Result of coefficient of determination (R^2) shows that averagely Landsat-8 estimated depths represented 57% of actual reference depth of the study area while Sentinel MSIL2A could define 46% the reference (SBES) depths.

Though log linear models based on multi-linear regression of several bands have yielded good results (Saeed *et al.*, 2021), in this study, linear regression of red band yielded better results compared to multi-spectral bands. Utilization of red band as optimal band for Lyzenga linear band model was also adopted by Casal *et al*. (2018) in estimating bathymetry of Irish waters using Sentinel-2 data. This shows that the use of longer wavelengths (*e.g.* red) for bathymetry in turbid waters is practicable than blue and green bands. Thus, estimated depths with red band showed higher correlation with reference depths than the blue and green bands.

The assertion by Amrari *et al*. (2021) that "bands with a longer wavelength are completely attenuated after few meters (or less) under the surface, and subsequently, the backward signal is insignificant" was contrary to the results obtained in this study. This was because, the long wavelength (red) band yielded bathymetry that closely depict bathymetry from the field data. Comparison of single band (red) Lyzenga model derived bathymetry from Landsat 8 in our study with that of multi linear band model of Dewi *et al*. (2021), show better RMSE (1.7 m) than was obtained in Dewi *et al*. (2021) with RMSE of 2.431 m. This also hold for Sentinel-2 as Dewi *et al*. (2021) recorded RMSE of 2.893 against 1.9 m obtained in this research. Worthy of mentioning is the fact that cloud is a serious factor in tropical equatorial regions when considering optical satellite data (Purkis *et al*., 2019; Daly *et al*., 2020). Hence, satellite data were not devoid of cloud. Landsat-8 L1TP and L2SP had 2.06% of cloud each, while Sentinel MS1LA had 32.60% cloud cover. This greatly impacted on the bathymetry derived from Sentinel-2 data despite its high spatial resolution. However, atmospheric correction of Landsat-8 level-1 of December 19th 2021 with C2RCC proved very effective in removing sunglint and radiometric noise from the satellite data (Casal *et al*., 2018).

4.0. Conclusions

The aim of this study was to estimate bathymetry for Imo River using medium resolution satellite images for the purpose of evaluating their performances and suitability. Landsat-8 level-1 and level-2 images and Sentinel-2 level- 2 images were used in the study. Stumpf *et al*. (2003) log ratio and Lyzenga *et al*. (2006) log linear empirical models were adopted. Blue, green and red image bands and a combination of the three bands were employed in the estimation process to allow for effective evaluation. For Lyzenga model, the best bathymetry output from the two images were obtained from the red band, while blue/red band ratio yielded more precise result from Landsat-8 level-1 based on Stumpf's model. Results from the blue/green band of both Landsat-8 level-2 and Sentinel-2 level-2 images closely depict field-based situation.

Research results further revealed that satellite images acquired on January 24, 2021 and February 18, 2021 (period within which sounding data used for calibration was carried out), were replete with cloud and not suitable for bathymetry estimation. Although these images were subjected to atmospheric correction, sun-glint removal and low pass filtering, range of estimated depth were beyond sounded depths. Sentinel-2 level-2 of January 24, 2021 estimated deep waters as shallow depths, and regions of low depth values as deep waters. On the contrary, Landsat-8 image of December 19, 2021 and Sentinel-2 image captured on December 20, 2021 yielded bathymetry outputs of good correlation with in-situ depths. Coefficient of determination shows that Landsat-8 averagely estimated depths by 57% while Sentinel-2 showed 46% performance. Deepest estimated depth from both satellites images was approximately 10 m compared to 12 m depth obtained from field-based sounding.

In conclusion, the study revealed that Landsat-8 and Sentinel-2 medium resolution images performed relatively similarly in bathymetry estimation of Imo River. Sentinel-2 generated depth deeper than Landsat-8 by 0.51 m and shallowest depth beyond Landsat-8 by 1.59 m but with low fidelity.

References

Ahola, R., Chénier, R., Sagram, M., and Horner, B. (2020). The impact of sensors for satellite derived bathymetry within the Canadian Arctic. *Geomatica*, (74), pp. 46–64.

Amadi, A.N., Olasehinde, P.I., Yisa, J., Nwankwoala, H.O., Ameh, M.I. and Shaibu, I. (2016). Analytical studies on heavy metal contamination of Imo river. INCEDI, Conference Accra, Ghana 805 [online]. Available at: https:/www.researchgate.net/publication/311713687_ANALYTICAL_STUDIES_ON_HEAVY_METAL_CONTAMINATION_OF_IMO_RIVER [Accessed 21 Nov. 2019].

Ashphaq, M., Srivastava, P.K. and Mitra, D. (2021). Review of near-shore satellite derived bathymetry: classification and account of five decades of coastal bathymetry research. *Journal of Ocean Engineering and Science* (2021). [online]. Available at: https://doi.org/10.1016/j.joes.2021.02.006. [Accessed 7 June 2020].

Cahalane, A.M., Monteys, X., Casal, G., Hanafin, J. and Harrisg, P. (2019). A comparison of Landsat 8, RapidEye and Pleiades products for improving empirical predictions of satellite-derived bathymetry. *Remote Sensing of Environment*, 233 (2019), pp. 111414.

Casal, G., Monteys, X., Hedley, J., Harris, P., Cahalane, C., and McCarthy, T. (2018). Assessment of empirical algorithms for bathymetry extraction using Sentinel-2 data. International *Journal of Remote Sensing*, (2018), pp. 1-25. [online]. Available at: https://doi.org/10.1080/01431161.2018.1533660 [Accessed 2 Feb. 2021].

Casal, G., Harris, P., Monteys, X., Hedley, J., Cahalane, C., and McCarthy, T. (2019). Understanding satellite-derived bathymetry using Sentinel 2 imagery and spatial prediction models. *GIScience & Remote Sensing*, 57 (3), pp. 271-286.

Caballero, I and Stumpf, R.P. (2020) Atmospheric correction for satellite-derived bathymetry in the Caribbean waters: from a single image to multi-temporal approaches using Sentinel-2A/B. Optics Express, 28(8), pp. 11742-11766.

Chukwuma, O.M. (2014). The characteristics of inland water transport in Nigeria. *IOSR Journal of Humanities and Social Science*, 19 (3), pp. 119-126.

Copernicus Open Access Hub. (No date). [online]. Available at: https://scihub.copernicus.eu. [Accessed 28 Feb. 2020].

Dewi, R.S., Rizaldy, A., Hartanto, P. and Suprajaka, S. (2021). Assessing the accuracy of shallow water depth estimation by using multispectral satellite images. *Geographia Technica*, 16 (Special Issue), pp. 180 - 197.

Daly, C., Baba, W. M., Bergsma, E. W. J., Almar, R. and Garlan, T. (2020, in preparation). The new era of regional coastal bathymetry from space: A showcase for West Africa using Sentinel-2 imagery. *Remote Sensing of Environment, 11*, (2020), pp. 1-20.

Dierssen, H. M. and Theberge, A.E. (2014). Bathymetry: assessing methods. *Encyclopedia of Natural Resources*. DOI: 10.1081/E-ENRW-120048588

Ekpa, A.U. and Ojinnaka, O.C. (2018). Estimating bathymetry of Cross River in Nigeria using remote sensing technique. *SSRG International Journal of Geoinformatics and Geological Science*, 5 (3), pp. 20 - 32.

El-Mewafi, M., Salah, M. and Fawzi B. (2018). Assessment of optical satellite images for bathymetry estimation in shallow areas using artificial neural network model. *American Journal of Geographic Information System* 2018, 7(4), pp. 99-106.

El-Sayed, M.S. (2018). Comparative study of satellite images performance in mapping lake bathymetry: Case study of Al-Manzala Lake, Egypt. American Journal of Geographic Information System, 7(3), pp. 82-87.

EOMAP GmbH & Co. KG (2013). Great Barrier Reef Bathymetry Survey 1-26. [online]. Available at: https://www.eomap.com/exchange/pdf/EOMAP_GBR_Bathymetry.pdf. [Accessed 23. January 2020].

Evagorou, E., Argyriou, A., Papadopoulos, N., Mettas, C., Alexandrakis, G. and Hadjimitsis, D. (2022). Evaluation of satellite-derived bathymetry from high and medium-resolution sensors using empirical methods. Remote Sensing, 14 (2022), pp. 772.

Gabr, B., Ahmed, M., and Marmoush, Y., (2020). PlanetScope and Landsat 8 Imageries for Bathymetry Mapping. *Journal of Marine Science and Engineering*, 8 (143); Doi:10.3390/jmse8020143.

Gao, J. (2009). Bathymetric mapping by means of remote sensing: methods, accuracy and limitations. *Progress in Physical Geography*, 33(1), pp. 103–116.

GEBCO Cookbook (2019). The IHO-IOC GEBCO Cook Book --- IHO Publication B-11 IOC Manuals and Guides, 6. [online]. Available at: https://www.star.nesdis.noaa.gov/socd/lsa/GEBCO_Cookbook/documents/CookBook_20191031.pdf [Accessed 16 April 2023].

Hashim, N.S., Windupranata, W., Tahar, K.N. and Sulaiman, S.A. (2021). Shallow-water bathymetry estimation at Pantai Tok Jembal, Terengganu, Malaysia using Landsat 8 (OLI). *IOP Conf. Series: Earth and Environmental Science* (2021), pp. 012008.

Hedley, J.D., Harborne, A.R. and. Mumby, P.J. (2005). Simple and robust removal of sun glint for mapping shallow-water benthos. *International Journal of Remote Sensing*, 26(10), pp. 2107–2112.

Holman, K. (2020). *Testing approaches and sensors for satellite-derived bathymetry in Nunavut*. MSc Thesis. University of Ottawa, Canada, 8979p.

International Hydrographic Organization, IHO (2019). Hydrographic information driving marine knowledge: IHO input to the report of the UN Secretary General on oceans and law of the sea. [online]. Available at: https://www.un.org/Depts/los/general_assembly/contributions_2019/IHOEN.pdf [Accessed 10 Nov. 2019].

Jawak, S.D., Vadlamani, S.S. and Luis, A.J. (2015). A synoptic review on bathymetry information using remote sensing technologies: Models, methods and comparisons. *Advances in Remote Sensing*, 4, pp. 147-162.

Jagalingam, P., Akshaya, B.J. and Hegde, A.V. (2015). Bathymetry mapping using Landsat-8 satellite imagery. *Procedia Engineering*, *116* (2015), pp. 560 – 566.

Jaelani, L. M.; Bobsaid, M. W. and Khomsin (2019). Bathymetric mapping of shallow water using Landsat 8 and Sentinel 2A Satellite data. case study: East Madura's Waters. IOP Conference Series: Earth and Environmental Science 389 (2019), pp. 012007.

Kimeli, A., Thoya, P., Ngisiang'e, N., Ong'anda, H. and Magori, C. (2018). Satellite-derived bathymetry: A case study of Mombasa Port Channel and its approaches, Kenya. *Western Indian Ocean Journal of Marine Science, 17* (2), pp. 93-102.

Khondoker, S.I., Siddiquee, Z.H. and Islam, A. (2017). The challenges of river bathymetry survey using space borne remote sensing in Bangladesh. *International Journal of Atmospheric and Oceanic Sciences*, 1(1), pp. 7-13.

Lee, K.R. (2012). *Using multi-angle Worldview-2 imagery to determine ocean depth near Oahu, Hawaii*. MSc Thesis. Naval Postgraduate School, Monterey, California.

Liu, Y., Zhao, J., Deng, R., Liang, Y., Gao, Y., Chen, Q., Xiong, L., Liu, Y., Tang, Y. and Tang, D. (2021). A downscaled bathymetric mapping approach combining multitemporal Landsat-8 and high spatial resolution imagery: Demonstrations from clear to turbid waters. *ISPRS Journal of Photogrammetry and Remote Sensing*, 180 (2021), pp. 65–81.

Lyzenga, D.R., Malinas, N.P., and Tanis, F.J. (2006). Multispectral bathymetry using a simple physically based algorithm. *IEEE Transactions on Geosciences and Remote Sensing*, 44, pp. 2251–2259.

LSDS-1619 (March 2022). Landsat 8-9 Collection 2 (C2) Level 2 Science Product (L2SP) Guide. Version 4.0. Department of the Interior- U.S. Geological Survey. [online]. Available at: https://d9-wret.s3.us-west-2.amazonaws.com/assets/palladium/production/s3fs-public/media/files/LSDS-1619_Landsat-8-9-C2-L2-ScienceProductGuide-v4.pdf. [Accessed 18 2023].

Muzirafuti, A., Barreca, G., Crupi, A., Faina, G., Paltrinieri, D., Lanza, S. and Randazzo, G. (2020). The contribution of multispectral satellite image to shallow water bathymetry mapping on the coast of Misano Adriatico, Italy. *Journal of Marine Science and Engineering*, 8 (126). Doi:10.3390/jmse8020126.

Okorie, D.O. and Nwosu, P.O. (2014). Seasonal variations in physico-chemical of Imo River. *IOSR Journal of Pharmacy and Biological Sciences*, 9 (5), pp. 07-09.

Oyo-Ita, I.O. and Oyo-Ita, O.E. (2017). Historical trend of polycyclic aromatic hydrocarbons contamination in recent dated sediment cores from the Imo River, Southeast Nigeria. *World Journal of Research and Review*, 5 (4), pp. 05-24.

Poti, M., Kinlan, B. and Menza, C. (2012). Bathymetry, pp. 9 - 32 in A biogeographic assessment of seabirds, deep sea corals and ocean habitats of the New York Bight: Science to Support Offshore Spatial Planning. NOAA Technical Memorandum NOS NCCOS 141 edited by Menza, C., Kinlan, B.P., Dorfman, D.S., Poti, M., Caldow, C. Silver Spring, MD.

Purkis, S.J., Gleason, A. C.R., Purkis, C.R., Dempsey, A. C., Renaud, P.G., Faisal, M., Saul, S. and Kerr, J.M. (2019). High-resolution habitat and bathymetry maps for 65,000 Sq. Km of Earth's remotest coral reefs. *Coral Reefs*, 38 (2019), pp. 467 - 488.

Revenga, C. and Y. Kura. (2003). Status and trends of biodiversity of inland water ecosystems. [online]. Available at: https://www.cbd.int/doc/publications/cbd-ts-11.pdf. [Accessed 5 April 2021].

Rossi, L., Mammi, I. and Pelliccia, F. (2020). UAV-derived multispectral bathymetry. *Remote Sensing*, (12), pp. 3897.

S2-PDGS-MPC-L2A-PFS-V14.2 (2017-06-23). S2 MPC Level 2A product format specification ref. [online] http://step.esa.int/thirdparties/sen2cor/2.4.0/Sen2Cor_240_Documenation_PDF/S2-PDGS-MPC-L2A-PDD-V14.2_V4.6.pdf [Accessed 18 Feb. 2023].

Saeed, R., Abdelrahman, S.M. and Negm, A. (2021). Satellite-derived bathymetry using Landsat-8 imagery for Safaga coastal zone, Egypt. *Acta Marisiensis Seria Technologica*, 18 (XXXV) 1, pp. 8 - 15.

Said, N. MD, Mahmud, M.R. and Hasan, R.C. (2017). Satellite-derived bathymetry: accuracy assessment on depths derivation algorithm for shallow water area. *The International Archives of the Photogrammetry, Remote Sensing and Spatial Information Sciences*, XLII-4/W5 (2017), pp. 159 – 164.

Schmitt, M. (2020). Potential of large-scale inland water body mapping from Sentinel-1/2 data on the example of Bavaria's Lakes and Rivers. *Springer*, 88, pp. 271–289.

Stumpf, R.P., Holderied, K. and Sinclair, M. (2003). Determination of water depth with high-resolution satellite imagery over variable bottom types. *Limnology Oceanography*, 48, pp. 547-556.

Tang, K.K.W. and Pradhan, B. (2015). Converting digital number into bathymetric depth: A case study over coastal and shallow water of Langkawi Island, Malaysia. FIG Working Week. No. 7505., Sofia, Bulgaria, 14p.

Traganos, D., Poursanidis, D., Aggarwal, B., Chrysoulakis, N. and Reinartz, P. (2018). Estimating satellite-derived bathymetry (SDB) with the Google earth engine and Sentinel-2. *Remote Sensing*, 10 (859): Doi:10.3390/rs10060859.

United States Geological Survey – Earth Explorer (No date). [online]. Available at: https://earthexplorer.usgs.gov [Accessed 2 Feb. 2022].

Vanderstraete, T., Goossens, R. and Ghabour, T.K. (2003). Remote sensing as a tool for bathymetric mapping of coral reefs in the Red Sea (Hurghada – Egypt). [online]. Available at: https://doi.org/10.4000/belgeo.16652. [Accessed 5 April 2021].

Yunus, A.P., Dou, J., Song, X. and Avtar, R. (2019). Improved bathymetric mapping of coastal and lake environments using Sentinel-2 and Landsat-8 images. *Sensors*, 19 (12), pp. 2788.

Zandbergen, S. (2020). *Multi-case evaluation of empirical methods for satellite-derived bathymetry*. Master Thesis. Delft University of Technology - TU Delft, the Netherlands, 83p.

Cite this article as:

Ekpa, A.U, Udoh, I.B. and Eyoh, A.E., 2023. Performance Evaluation of Medium Resolution Satellite Images in Bathymetry Estimation for Imo River. *Nigerian Journal of Environmental Sciences and Technology*, 7(3), pp. 435-451. https://doi.org/10.36263/nijest.2023.03.0434